Structure of a High Karlovitz n-C_7H_{16} Premixed Turbulent Flame

Bruno Savard[a,*], Brock Bobbitt[b], Guillaume Blanquart[b]

[a] *Graduate Aerospace Laboratories,* [b] *Department of Mechanical Engineering,*

California Institute of Technology, Pasadena, CA 91125, USA

[*] Corresponding author

Mailing address: 1200 E. California Blvd, MC 205-45, Pasadena, CA, USA 91125

Fax: (626) 568-2719

Email address: **bsavard@caltech.edu**

Colloquium: Turbulent Flames

Total length of paper: 6188 words (Method 2)

Detailed word count

Maint text: 4192

References: 515

Table 1: 194	Figure 4: 180
Figure 1: 134	Figure 5: 128
Figure 2: 106	Figure 6: 143
Figure 3: 134	Figure 7: 462

Abstract

Results from a series of direct numerical simulations (DNS) of a high Karlovitz, slightly lean ($\phi = 0.9$), *n*-C_7H_{16}/air premixed turbulent flame are presented. The flame is statistically flat and is subjected to an inflow of homogeneous isotropic turbulence. A 35-species and 217-reaction mechanism [Bisetti *et al.* Combust. Flame 159 (2012) 317-335] is used to represent the chemistry. Two simulations have been performed: one with unity Lewis number to asses the effects of turbulence on the flame structure in the absence of differential diffusion, and the other with non-unity Lewis numbers to analyze how turbulence affects differential diffusion. The Karlovitz numbers are 280 and 220 respectively. The first simulation reveals that the flame is strongly affected by turbulence as enhanced mixing largely thickens the preheat zone. However, the turbulent flame structure (*i.e.* the correlation between species and temperature) is similar to that of a one-dimensional flat flame, suggesting that turbulence has limited effet on the flame in temperature space, in the absence of differential diffusion. In the second simulation, the flame structure is affected by turbulence, as differential diffusion effects are weakened. It is suggested that this result is attributed to the fact that turbulence drives the effective species Lewis numbers towards unity through an increase in effective species and thermal diffusivities. Finally, the reaction zones of both the unity and the non-unity Lewis number turbulent flames remain thin, and are locally broken (only to some extent for the unity Lewis number flame, and more strongly for non-unity).

Keywords: Premixed turbulent flame, detailed finite-rate chemistry, differential diffusion, direct numerical simulation, heptane.

1. Introduction

As industrial applications of turbulent premixed (and partially premixed) flames fall in the thin/broken reaction zones regimes, understanding how a flame behaves in these regimes is critical [1]. These regimes are characterized by a large Karlovitz number which is defined as the ratio of the flame time to the Kolmogorov time, *i.e.* $Ka = t_F/t_\eta$. Experiments are difficult to conduct at high Karlovitz numbers and a limited number of them are available in the literature [2, 3]. Equivalently, due to their expensive computational costs, very few direct numerical simulations (DNS) of turbulent premixed flames in the broken reaction zones or the thin reaction zones regimes have been performed [4–8]. Figure 1 presents all of these simulations (to the best of the authors' knowledge) in the context of the regime diagram (as proposed by Peters [9]). Note that only simulations performed with detailed finite-rate

chemistry are presented (an additional study in the context of astrophysics can be found in Ref. [10]).

[Fig. 1 about here.]

The only fuels that have been considered in previous simulations are hydrogen [4, 7], methane [5, 6], and propane [5]. While these fuels are used in several ground-based applications [11], most of the fuels used for transportation contain larger hydrocarbons [12]. Since their chemical pathways are far more complex, and a wide range of stable species are present through the flame front, it remains unclear how turbulence influences their chemistry at high Karlovitz number.

Moreover, heavy hydrocarbons have large Lewis numbers (*e.g.* $Le_{\mathrm{C_{12}H_{26}}} \approx 3.5$). It has also been observed that for sufficiently high Karlovitz number differential diffusion effects were negligible for both H_2 ($Le_{\mathrm{H_2}} \approx 0.3$) and C_3H_8 ($Le_{\mathrm{C_3H_8}} \approx 2$) [5]. However, this similar behavior between smaller and larger than unity Lewis number fuels cannot be generalized to lower Karlovitz numbers, as pertinent to the transition between the thin/broken reaction zones regimes. Furthermore, while the series of lean H_2/air premixed flames performed by Aspden *et al.* [4] have provided information on how turbulence affects differential diffusion over a wide range of Karlovitz numbers [13], there is no such information available for heavy hydrocarbon fuels.

To tackle these questions, a series of DNS of a premixed *n*-C_7H_{16} turbulent flame close to the transition between the thin/broken reaction zones regimes is presented in this paper. A first simulation with unity Lewis number is performed in order to assess the effect of turbulence on the flame structure in the absence of differential diffusion. A second simulation with non-unity Lewis numbers (amongst which $Le_{\mathrm{C_7H_{16}}} = 2.8$) is performed to study how turbulence affects differential diffusion.

The paper is organized as follows. In Section 2, the numerical approach is presented. The results are presented in Section 3; and Section 4 contains the conclusion.

2. Numerical approach

The flow configuration is first introduced, followed by the equations solved. Finally, the turbulence forcing method is described.

2.1. Flow configuration

Figure 2 presents a schematic diagram of the flow configuration. A statistically-flat flame was chosen in order to isolate the effects of turbulence on the flame from mean shear effects. Furthermore, since both an inflow and an outflow are present, the simulation can be run for an unbounded arbitrary time, allowing the turbulent flame to reach a statistically-stationary state.

[Fig. 2 about here.]

The unburnt gas is a slightly lean ($\phi = 0.9$) *n*-C_7H_{16}/air mixture at standard temperature ($T_u = 298$ K) and pressure ($P_0 = 1$ atm). These standard conditions were chosen in order to match the experimental conditions of most premixed turbulent flames. Two simulations are performed: one with non-unity Lewis numbers and one with unity. The parameters for both simulations are presented in Table 1. Given this choice of unburnt conditions, the other parameters were chosen to maximize the Karlovitz number, while keeping a sufficiently large l/l_F, where l is the integral length scale and l_F is the laminar flame thickness. The Karlovitz number is defined as the ratio of the flame time scale to the Kolmogorov time scale, *i.e.* $Ka = t_F/t_\eta = (l_F/S_L)\,(\epsilon/\nu)^{1/2}$, where S_L is the laminar flame speed, ϵ is the dissipation rate, and ν is the mixture kinematic viscosity. The Karlovitz numbers chosen are sufficiently high that these two flames are expected to fall at the transition between the thin/broken reaction zones regimes (see Fig. 1).

[Table 1 about here.]

The turbulent flame speed is not known *a priori*. A first simulation was performed with tabulated chemistry [14] (unity Lewis number) to obtain an estimate of the turbulent flame speed. The flame was allowed to slightly drift for more than a hundred eddy turnover times, 100τ. From this simulation, the turbulent flame speed was estimated and the inlet velocity was changed to match this estimate. Then, the finite-rate chemistry simulations were started from the statistically steady (tabulated) simulation. The simulations were performed for 10τ, almost two flame brush through times. The data was collected over the next 15τ. The unity Lewis number flame drifted by less than $0.1L$ from its initial position ($x = 3.5L$), and the non-unity Lewis number flame by less than $0.3L$.

The simulated flame is characterized by an important velocity ratio u'/S_L (about 20), where u' is the rms velocity fluctuation. This is a direct consequence of the large Karlovitz number. Consequently, a special treatment has to be applied to the inlet and the outlet in order to avoid negative inflow/outflow velocities (for numerical stability). The unburnt gas is injected with a low turbulent kinetic energy (TKE), such that there are no negative axial velocities. This inflow is generated from a separate homogenous isotropic turbulence simulation. Velocity fields forcing (subsection 2.3) maintains this low TKE over a distance of $0.5L$, after which the forcing magnitude is increased such that the TKE reaches the desired value. This nominal velocity fields forcing is stopped after a distance of $8L$, allowing the turbulence to decay sufficiently that there are no negative axial velocities at the outlet. The forcing method used is described in subsection 2.3.

2.2. Governing equations

The low Mach number Navier-Stokes equations are considered. Conservation of mass reads

$$\frac{\partial \rho}{\partial t} + \nabla \cdot (\rho \boldsymbol{u}) = 0, \tag{1}$$

where ρ is the mixture density and $\boldsymbol{u}$ is the velocity. Conservation of momentum is expressed as

$$\frac{\partial}{\partial t}(\rho \boldsymbol{u}) + \nabla \cdot (\rho \boldsymbol{u} \otimes \boldsymbol{u}) = -\nabla p + \nabla \cdot \boldsymbol{\sigma} + \boldsymbol{f}, \tag{2}$$

where p is the hydrodynamic pressure, $\boldsymbol{f}$ is a forcing term used to maintain the presence of turbulent fluctuations (see subsection 2.3), and

$$\boldsymbol{\sigma} = \mu \left(\nabla \boldsymbol{u} + \nabla \boldsymbol{u}^{\top} \right) - \frac{2}{3} \mu (\nabla \cdot \boldsymbol{u}) \mathbf{I}, \tag{3}$$

where μ is the mixture dynamic viscosity and $\mathbf{I}$ is the identity tensor. A transport equation is solved for each species i

$$\frac{\partial}{\partial t}(\rho Y_i) + \nabla \cdot (\rho \boldsymbol{u} Y_i) = -\nabla \cdot \boldsymbol{j_i} + \dot{\omega}_i, \tag{4}$$

where Y_i is the species mass fraction, $\dot{\omega}_i$ is the species production rate, and $\boldsymbol{j_i}$ is the species diffusion mass flux. The latter takes the following form

$$\boldsymbol{j_i} = -\rho D_i \frac{Y_i}{X_i} \nabla X_i - \rho Y_i \boldsymbol{u_c}, \tag{5}$$

where X_i is the species mole fraction and D_i is the mixture species diffusivity [15]. A correction velocity $\boldsymbol{u_c} = -\sum D_i \frac{Y_i}{X_i} \nabla X_i$ is present to ensure zero net diffusion mass flux [16]. The following form of the temperature equation is solved

$$\begin{aligned} \frac{\partial}{\partial t}(\rho T) + \nabla \cdot (\rho \boldsymbol{u} T) &= \nabla \cdot (\rho \alpha \nabla T) + \dot{\omega}_T \\ &- \frac{1}{c_p} \sum_i c_{p,i} \boldsymbol{j_i} \cdot \nabla T + \frac{\rho \alpha}{c_p} \nabla c_p \cdot \nabla T, \end{aligned} \tag{6}$$

where T is the temperature, $c_{p,i}$ is the species heat capacity, c_p is the mixture heat capacity, $\alpha = \lambda / (\rho c_p)$ is the mixture thermal diffusivity, where λ is the mixture thermal conductivity, and $\dot{\omega}_T$ is the temperature production term. The latter can be expressed as $\dot{\omega}_T = -\frac{1}{c_p} \sum h_i(T) \dot{\omega}_i$, where h_i is the species enthalpy at temperature T. Finally,

the equation of state for a mixture of perfect gases is considered

$$P_0 = \frac{\rho R T}{W}, \tag{7}$$

where P_0 is the thermodynamic pressure, R is the universal gas constant, and W is the mixture molar weight.

The species and enthalpy production terms are taken from a reduced, *n*-heptane chemical model which contains 35 species and 217 elementary reactions (forward and backward rates counted separately) [17]. As the gas mixture is slightly lean, all aromatic species (and associated reactions) were removed.

The species viscosities μ_i are computed by standard kinetic theory [18] and the mixture viscosity μ is calculated using Wilke's formula [19]. The mixture thermal conductivity is obtained following Mathur *et al.* [20], where the species thermal conductivities λ_i are computed by Eucken's formula [21]. In order to reduce the computational cost of the simulation, the species diffusivities are computed as $D_i = \alpha / Le_i$, with the Lewis numbers Le_i assumed to be constant throughout the flame. For the non-unity Lewis number simulation, these species Lewis numbers Le_i are extracted from the simulation of a one-dimensional, laminar premixed flame with full transport properties, using FlameMaster [22]. The Lewis numbers are evaluated at a temperature corresponding to the beginning of the reaction zone such that deviations from the full transport solution are negligible.

Equations 1 to 7 are solved numerically using the energy conservative, finite difference code NGA designed for the simulation of variable density low Mach number turbulent flows [23]. The scheme used is second-order accurate in both space and time. A semi-implicit Crank-Nicolson time integration is used. The third-order Bounded QUICK scheme, BQUICK [24], is used as the scalar transport scheme to ensure the transported species mass fractions and temperature remain within their physical bounds.

2.3. Turbulence forcing

The decay of the TKE in the absence of velocity field forcing can be estimated from theory by analogy to decaying isotropic turbulence, considering $\mathrm{d}k/\mathrm{d}t = -k/\tau$, with τ the eddy turnover time ($\tau = k/\epsilon$). With U the mean bulk/inlet velocity, the characteristic length scale over which the TKE decays is $U\tau = 0.1$mm, which is too small compared to the laminar flame thickness (see Table 1). As a consequence, the use of velocity field forcing is necessary. In previous work, spectral forcing techniques were often used to offset the decay of TKE and maintain the turbulence characteristics [4, 25]. In this work, the linear velocity forcing method [26–28] was preferred for its more physical nature and good stability properties [29]. The method is adapted to take into account the axially

evolving nature of the flow. Consequently, the forcing term $\boldsymbol{f}$ in Eq. 2 takes the following form

$$\boldsymbol{f}\left(x,y,z,t\right)=A\frac{k_0}{k\left(x,t\right)}\left(\rho\left(x,y,z,t\right)\boldsymbol{u}\left(x,y,z,t\right)-\overline{\rho\boldsymbol{u}}\left(x,t\right)\right), \tag{8}$$

where A is the forcing coefficient (computed as in Ref. [29]), which takes the form of the inverse of a time scale, k_0 is the desired TKE, and k is the planar Favre-averaged TKE, defined as

$$k=\frac{1}{2}\left(\widetilde{\left(u''\right)^2}+\widetilde{\left(v''\right)^2}+\widetilde{\left(w''\right)^2}\right). \tag{9}$$

The planar Favre average is defined as

$$\widetilde{\boldsymbol{\phi}}=\frac{\overline{\rho\boldsymbol{\phi}}}{\overline{\rho}}, \tag{10}$$

with the standard planar average

$$\overline{\boldsymbol{\phi}}\left(x,t\right)=\frac{1}{L^2}\int_0^L\int_0^L\boldsymbol{\phi}\left(x,y,z,t\right)\mathrm{d}y\mathrm{d}z. \tag{11}$$

Note that while the present configuration misses the generation of turbulence due to large scale flow straining (larger than the domain size), the linear forcing method *mimics* this large scale straining by appending a source term to the momentum equation (Eq. 8) [26, 27].

With the forcing method used, homogeneous isotropic turbulence is imposed upstream of the flame. A slight decrease in the TKE through the flame and a relaxation back to the imposed TKE further downstream was found (not shown). This evolution is consistent with the experimental results of Cheng *et al.* [30]. While the trends agree, in both studies the variations in TKE through the flame remain marginal, which has also been observed computationally [6]. Consistently, the TKE was enforced to be constant through the flame in previous numerical studies using velocity field forcing [4, 25].

3. Effects of the turbulence on the flame

The simulation performed with unity Lewis number is analyzed first to assess the effects of turbulence on the flame structure in the absence of differential diffusion. Then, the effects of turbulence on differential diffusion are presented. Finally, the reaction zones of both flames are analyzed.

3.1. Turbulent flame structure in the absence of differential diffusion

The effects of turbulence on the flame are illustrated in Fig. 3. Unsurprisingly, the flame looks very different

from a flamelet, *i.e.* the flame is not thin. The turbulent flame is visibly thicker than the laminar flame as turbulence enhances mixing and thickens the preheat zone. It is interesting to note that smaller turbulent structures are observed upstream of the flame (*i.e.* in the preheat zone) than close to the reaction zone. This is partially-explained by the fact that the kinematic viscosity increases (by up to a factor of 30) and the Kolmogorov length scale, $\eta = \left(\nu^3/\epsilon\right)^{1/4}$, increases through the flame by about a factor of 13.

[Fig. 3 about here.]

To properly assess the influence of turbulence on the flame structure, one can analyze the correlation between species and temperature (or any other progress variable). As such, the flame structure can be adequately compared to that of a one-dimensional laminar flame, which is well represented in temperature space.

In this sense, several species mass fractions are plotted against temperature and are compared to their one-dimensional laminar flame equivalent. Figure 4 shows joint probability densities of *n*-C_7H_{16}, C_2H_4, and CO_2 mass fraction, *vs.* temperature. These species correspond to a reactant, an intermediate species, and a product, respectively. The conditional mean of these species mass fraction (conditional on temperature) is also shown. This figure is representative of the overall flame structure as the mass fractions of other species show similar behaviors. These results suggest that the influence of turbulence on the flame strucutre in the absence of differential diffusion is very limited as the spread of the joint PDF is limited (this has also been observed by Aspden *et al.* for a high-Ka CH_4/air flame [5]). More interestingly, the conditional mean profiles of these species follow very closely the profiles of a one-dimensional, unstretched laminar flame at the same condition. This result is surprising as the turbulent flame is clearly not in the flamelet regime and does not look like a flamelet.

[Fig. 4 about here.]

Although the last result may be surprising, an expected first order effect of turbulence on species transport is the increase in the effective diffusivity through increased mixing. Assuming turbulence mixes all scalars the same way, the turbulent diffusivities (D_T) may be assumed equal for all of these scalars, and the effective diffusivity becomes

$$D_{\text{eff}} = D + D_T. \tag{12}$$

To assess the effect of diffusivity on the flame structure, additional laminar flamelet solutions were obtained varying this diffusivity. Whereas the resulting laminar flame speeds and flame thicknesses were accordingly altered by a factor of $(D_{\text{eff}}/D)^{1/2}$, the flame structure was virtually unaffected, as shown in Fig. 5. This might be the result

of the large separation between the diffusive and chemical time scales, thus explaining the negligible effect of turbulence on the flame structure.

[Fig. 5 about here.]

In summary, while the turbulent flame is thickened by turbulence and is clearly not a thin flame, its *structure* is similar to that of a flamelet. This may suggest that the use of a progress variable with tabulated chemistry [14, 31, 32] would be justified and sufficient even at such high Karlovitz number.

3.2. Turbulent flame structure with differential diffusion

Similarly to Fig. 4, Fig. 6 presents the structure of C_2H_4 through the non-unity Lewis number flame. The full-transport flamelet solution is also added for comparison. While turbulence has almost no impact on the structure of the unity Lewis number flame, it has a clear effect on that of a non-unity Lewis numbers flame. In this case, the turbulent flame structure lies between that of a full transport and a unity Lewis number flamelet. Once again, a first order effect of turbulence on scalar transport is an increase in the effective diffusivity of each scalar (including species mass fractions and temperature) through increased mixing. As a result, the effective species Lewis number take the following from

$$Le_{i,\mathrm{eff}} = \frac{\alpha + D_T}{D_i + D_T}. \tag{13}$$

A similar expression for these effective Lewis numbers was first suggested by Peters [9] and has been recently further analyzed and validated [13]. This suggests that if the turbulence were sufficiently intense, the non-unity Lewis number case would behave the same as the unity Lewis number case, *i.e.* turbulence would suppress differential diffusion effects.

[Fig. 6 about here.]

This behavior is observed at low temperatures (*i.e.* in the preheat zone), where the data from the DNS collapse perfectly with the unity Lewis number flamelet solution. However, at higher temperatures, the structure deviates from that of a unity Lewis number flamelet. This can be attributed to the fact that the Kolmogorov length scale grows through the flame, and therefore the "local Karlovitz number" is reduced. As a result, preferential diffusion effects may still be present, especially towards the reaction zone. These effects are disscussed in more details in the following subsection.

3.3. Reaction zone

Figure 7(a) and 7(b) show contours of the source term of *n*-C_7H_{16} and H_2O for the unity Lewis number flame. The turbulent reaction zone is locally of the same thickness as that of a one-dimensional flat flame. These plots suggest that the flame belongs to the thin reaction zones regime, which could seem inconsistent with the fact that the Kolmogorov length scale in the unburnt gases is 10 times smaller than the laminar reaction zone thickness. However, as mentioned already, the Kolmogorov length scale increases through the flame due to the increasing kinematic viscosity, and becomes as large as the laminar reaction zone thickness as it reaches the burnt side. It is also interesting to note that the *n*-C_7H_{16} consumption rate is at some locations smaller, suggesting that, while being thin, the reaction zone is *broken* to some extent. This is confirmed by Fig 7(c), which plots the source term of *n*-C_7H_{16} and H_2O normalized by their laminar value. Both of them deviate from their flamelet value; more for *n*-C_7H_{16} than for H_2O. These fluctutations are suspected to be a consequence of stretching, as observed in Ref. [33, 34].

Interestingly, while little deviations from the laminar flame structure were found (Fig. 4), the source terms fluctuate by up to 100% around the laminar value (Fig. 7(c)). Although the species mass fractions correlate very well with temperature, small deviations from the laminar profiles are present (see Fig. 4), especially around the peak fuel consumption temperature ($T = 1300$ K). These small absolute deviations from the laminar profiles can result in large relative fluctuations and hence large fluctuations in the chemical source terms.

[Fig. 7 about here.]

Fig. 7(d), 7(e), and 7(f) show the same plots but for the non-unity Lewis number flame. Once again, the reaction zone is locally of the same thickness as that of the flamelet solution. However, the non-unity Lewis number reaction zone shows more signs of local extinction, as illustrated by Fig. 7(d) and 7(f). It is important to note that the reaction zone is thin and broken at several locations, but not distributed. Finally, although the source term of H_2O fluctuates more in the non-unity than in the unity Lewis number flame, it still shows less signs of local extinction than the source term of *n*-C_7H_{16}.

It may be argued that the Karlovitz number is not sufficiently high to lead to a distributed reaction zone. Interestingly, Aspden *et al.* [4] have shown that a lean H_2/air flame could transition from a thin reaction zone to a distributed reaction zone behavior (as the Karlovitz number is increased) without showing signs of a broken reaction zone. These different observations may be due to the fact that H_2 has a Lewis number less than unity ($Le_{\mathrm{H_2}} \approx 0.3$), whereas *n*-$C_7H_{16}$ has a greater than unity Lewis number ($Le_{\mathrm{C_7H_{16}}} = 2.8$). A more diffusive flame may be expected to be more resistant to turbulent effects/perturbations.

Note that turbulence has an effect on the overall flame speed and leads to a significant increase ($S_T^{Le=1} = 3.7 S_L^{Le=1}$ and $S_T^{Le\neq1} = 1.9 S_L^{Le\neq1}$, with S_T the turbulent flame speed), consistent with previous work [35, 36]. The local extinction events observed for the non-unity Lewis number flame also have an effect as its turbulent flame speed was found to be smaller than that of the unity Lewis number flame, while its laminar flame speed is larger (see Table 1). Such a differential diffusion effect has been observed in previous experimental work [34, 37].

Finally, these interesting behaviors would not have been observed with a simpler fuel such as CH_4. This reinforces the idea that complex fuels need to be used more often in DNS of turbulent premixed flames.

4. Conclusions

A series of direct numerial simulations of a high Karlovitz number, *n*-C_7H_{16}, turbulent premixed flame have been performed. The effects of turbulence on the flame structure in the absence of differential diffusion have been assessed through a first simulation with unity Lewis number; whereas the effects of turbulence on differential diffusion have been analyzed through a second simulation with non-unity Lewis numbers.

The flame thickness of the unity Lewis number flame was shown to be largely affected by turbulence. However, its structure (defined as the dependence of species mass fractions on temperature) is very similar to that of a one-dimensional, flat flame, suggesting that turbulence has a very limited impact on the flame in temperature space, in the absence of differential diffusion. On the other hand, the structure of the non-unity Lewis number flame is affected more substantially by turbulence. It was argued that turbulence affects the flame structure through an effective Lewis number. At high turbulence levels (*i.e.* high Karlovitz number) turbulence reduces differential diffusion effects. These effects are almost supressed in the preheat zone, but are still present close to the reaction zone.

The reaction zone of both the unity and the non-unity Lewis numbers flames was shown to be thin and broken at various locations. Interestingly, the reaction zone was more broken in the non-unity Lewis number case. It was also observed that not all species' reaction zones are as strongly broken. This effect may be attributed to the larger than unity Lewis number of *n*-C_7H_{16}.

Acknowledgements

The authors gratefully acknowledge funding from the Air Force Office of Scientific Research (Award FA9550-12-1-0144) under the supervision of Dr. Chiping Li, and from the Natural Sciences and Engineering Research Council of Canada (NSERC Postgraduate Scholarship D), and the Department of Energy for access to the National Energy Research Scientific Computing Center.

References

[1] H. Pitsch, *Ann. Rev. Fluid Mech.* 38 (2006) 453–482.

[2] Y. Chen, R. Bilger, *Combust. Flame* 138 (2004) 155–174.

[3] J. Hult, S. Gashi, N. Chakraborty, M. Klein, K. Jenkins, S. Cant, C. Kaminski, *Proc. Comb. Inst.* 31 (2007) 1319–1326.

[4] A. Aspden, M. Day, J. Bell, *J. Fluid Mech.* 680 (2011) 287–320.

[5] A. Aspden, M. Day, J. Bell, *Proc. Comb. Inst.* 33 (2011) 1473–1480.

[6] R. Sankaran, E. Hawkes, J. Chen, T. Lu, C. Law, *Proc. Comb. Inst.* 31 (2007) 1291–1298.

[7] W. Wang, K. Luo, J. Fan, *Energ. Fuel* 27 (2013) 549–560.

[8] E. Hawkes, O. Chatakonda, H. Kolla, A. Kerstein, J. Chen, *Combust. Flame* 159 (2012) 2690–2703.

[9] N. Peters, *Turbulent Combustion*, Cambridge University Press, Cambridge, 2000.

[10] A. Aspden, J. Bell, S. Woosley, *Astrophys. J.* 710 (2010) 1654–1663.

[11] R. Cheng, D. Littlejohn, P. Strakey, T. Sidwell, *Proc. Comb. Inst.* 32 (2009) 3001–3009.

[12] M. Colket, T. Edwards, S. Williams, N. Cernansky, D. Miller, F. Egolfopoulos, P. Lindstedt, K. Seshadri, F. Dryer, C. Law, D. Friend, D. Lenhert, H. Pitsch, A. Sarofim, M. Smooke, W. Tsang, "Development of an experimental database and kinetic models for surrogate jet fuels" in *45th AIAA Aerospace Sciences Meeting and Exhibit* (Reno, Nevada) (Jan. 8-11 2007).

[13] B. Savard, G. Blanquart, *Combust. Flame* 161 (2014) 1547–1557.

[14] E. Knudsen, H. Pitsch, *Combust. Flame* 156 (2009) 678–696.

[15] R. Bird, W. Stewart, E. Lightwood, *Transport Phenomena*, John Wiley and Sons, New York, 1960.

[16] T. Coffee, J. Heimerl, *Combust. Flame* 43 (1981) 273–289.

[17] F. Bisetti, G. Blanquart, M. Mueller, H. Pitsch, *Combust. Flame* 159 (2012) 317–335.

[18] O. Hirschfelder, C. Curtiss, R. Bird, *Molecular Theory of Gases and Liquids*, John Wiley and Sons, New York, 1954.

[19] C. Wilke, *J. Chem. Phys.* 18 (4) (1950) 517–519.

[20] S. Mathur, P. Tondon, S. Saxena, *Mol. Phys.* 12 (6) (1967) 569–579.

[21] A. Eucken, *Phys. Z.* 14 (1913) 324–333.

[22] H. Pitsch, *FlameMaster: A C++ computer program for 0D combustion and 1D laminar flame calculations. Available at http://www.stanford.edu/∼hpitsch/.* (1998).

[23] O. Desjardins, G. Blanquart, G. Balarac, H. Pitsch, *J. Comput. Phys.* 227 (2008) 7125–7159.

[24] M. Herrmann, G. Blanquart, V. Raman, *AIAA Journal* 44 (2009) 2879–2886.

[25] A. Poludnenko, E. Oran, *Combust. Flame* 157 (2010) 995–1011.

[26] T. Lundgren, "Linear forced isotropic turbulence" in *Annual Research Briefs* (Center for Turbulence Research, Stanford) (2003) 461-473.

[27] C. Rosales, C. Meneveau, *Phys. Fluids* 17 (2005) 095106.

[28] P. Carroll, G. Blanquart, *J. Turbul.* 15 (2014) 429–448.

[29] P. Carroll, G. Blanquart, *Phys. Fluids* 25 (2013) 105114.

[30] R. Cheng, D. Littlejohn, W. Nazeer, K. Smith, *J. Eng. Gas Turb. Power* 130 (2008) 021501.

[31] J. van Oijen, F. Lammers, L. de Goey, *Combust. Flame* 127 (2001) 2124–2134.

[32] O. Gicquel, N. Darabiha, D. Thévenin, *Proc. Comb. Inst.* 28 (2000) 1901–1908.

[33] E. Hawkes, J. Chen, *Combust. Flame* 144 (2006) 112–125.

[34] D. Bradley, M. Lawes, K. Liu, M. Mansour, *Proc. Comb. Inst.* 34 (2013) 1516–1526.

[35] N. Chakraborty, R. Cant, *Combust. Flame* 158 (2011) 1768–1787.

[36] A. Poludnenko, E. Oran, *Combust. Flame* 158 (2011) 301–326.

[37] D. Bradley, P. Gaskell, X. Gu, A. Sedaghat, *Combust. Flame* 143 (2005) 227–245.

5. *

Tables and Figures

	unity Le	non-unity Le_i
Domain size	$L \times L \times 11L$	
L (m)	2.3×10^{-3}	
Grid	$128 \times 128 \times 1408$	
Δx (m)	1.8×10^{-5}	
η (m)	9×10^{-6}	
n_F	23	21
Δt (s)	8×10^{-8}	5×10^{-8}
ϕ	0.9	
S_L (m/s)	0.29	0.36
l_F (mm)	0.43	0.39
l/l_F	1.0	1.1
u'/s_L	21	18
$Ka = t_F/t_\eta$	280	220
$Re_t = (u'l)/\nu$	190	

Table 1: Parameters of the simulation. Δx is the grid spacing (uniform), η the Kolmogorov length scale in the unburnt gas, n_F the number of grid points through the laminar flame thickness, Δt the time step, ϕ the equivalence ratio, and Re_t the turbulent Reynolds number in the unburnt gases.

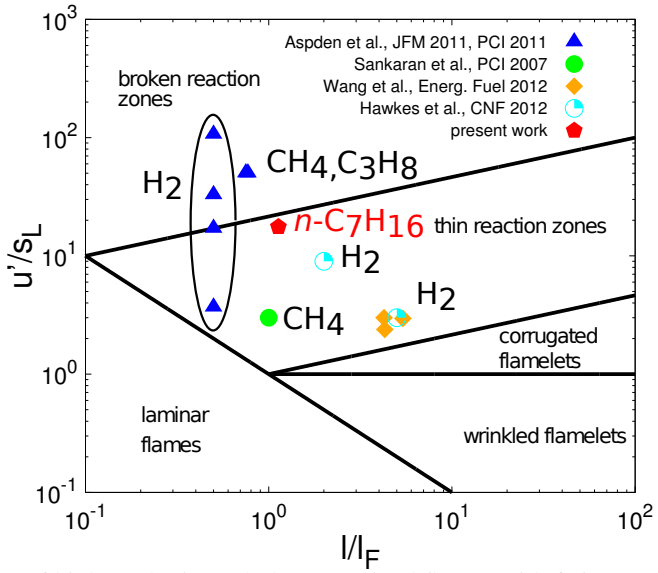

Fig. 1: DNS of high Karlovitz turbulent premixed flames with finite-rate chemistry.

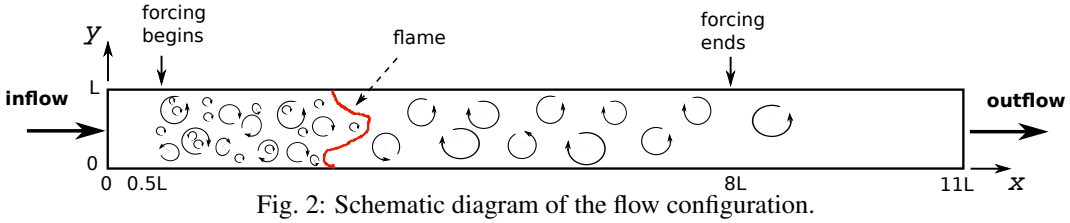

Fig. 2: Schematic diagram of the flow configuration.

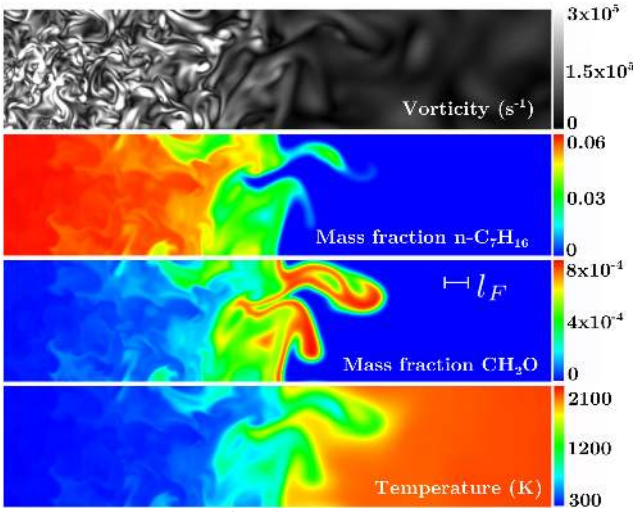

Fig. 3: Contours of vorticity, *n*-C_7H_{16} and CH_2O mass fractions, and temperature through the flame brush on a two-dimensional horizontal slice. The laminar flame thickness l_F is added for comparison.

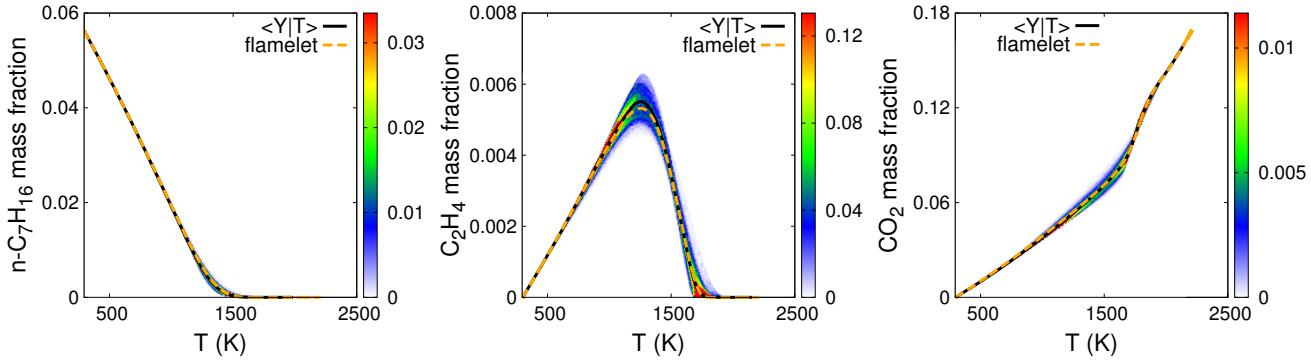

Fig. 4: Joint PDF and conditional mean (solid line) of the *n*-C_7H_{16} (left), C_2H_4 (center), and CO_2 (right) mass fraction *vs.* temperature from the unity Lewis number DNS. The unity Lewis number flamelet solution is also shown (dashed line).

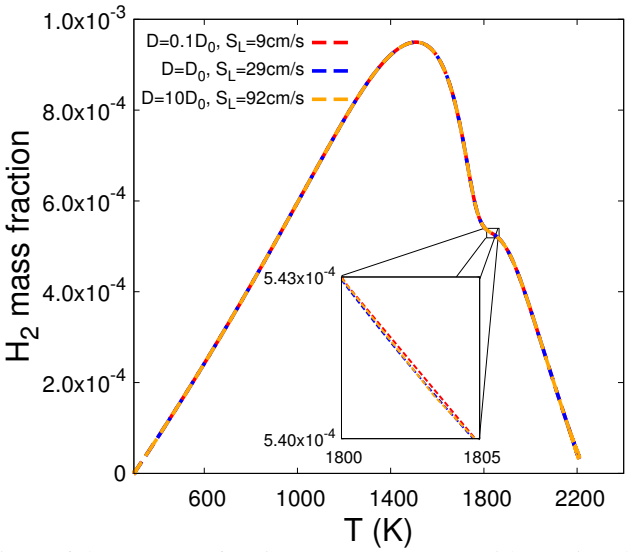

Fig. 5: Flamelet solutions of the H_2 mass fraction *vs.* temperature with varying diffusivity coefficients.

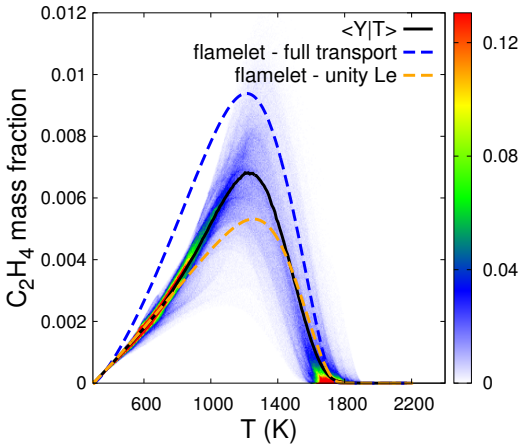

Fig. 6: Joint PDF and conditional mean (solid line) of the C_2H_4 mass fraction *vs.* temperature from the non-unity Lewis number DNS. The non-unity and unity Lewis number flamelet solutions are also shown (dashed line).

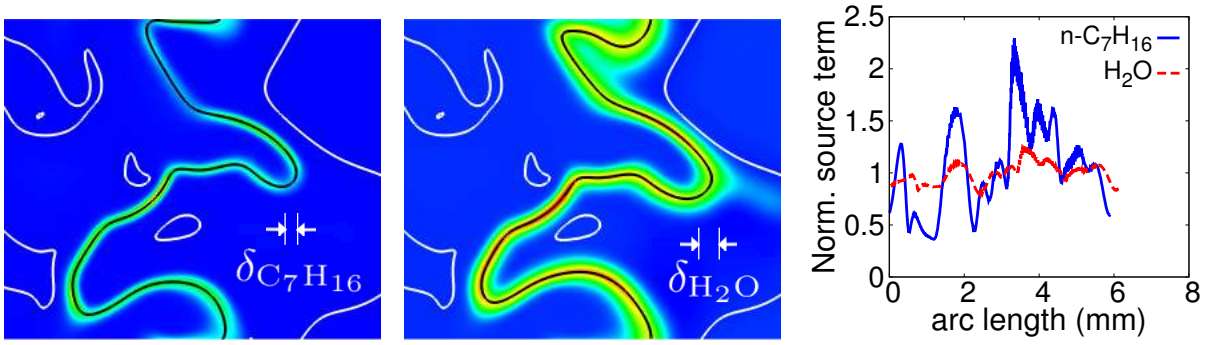

(a) $\dot{\omega}_{C_7H_{16}}$; $T_{\text{peak}} = 1364$ K (b) $\dot{\omega}_{H_2O}$; $T_{\text{peak}} = 1613$ K (c) $\dot{\omega}$ at T_{peak}

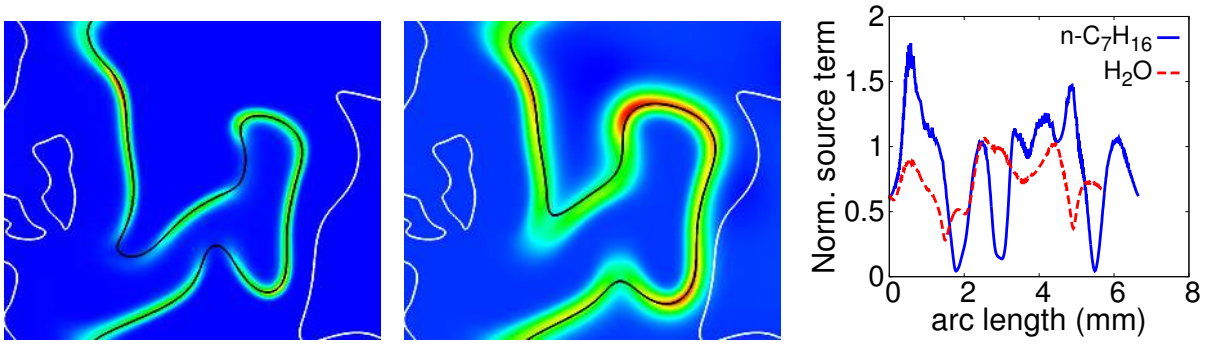

(d) $\dot{\omega}_{C_7H_{16}}$; $T_{\text{peak}} = 1240$ K (e) $\dot{\omega}_{H_2O}$; $T_{\text{peak}} = 1592$ K (f) $\dot{\omega}$ at T_{peak}

Fig. 7: (a,b,d,e) Contours of species source terms normalized by their laminar values on a two-dimensional horizontal slice. Also shown are three temperature isocontours: 600 K (white, left of the reaction zone), temperature of peak source term T_{peak} (black), and 1850 K (white, right of reaction zone). The laminar reaction zone thicknesses of *n*-C_7H_{16} and H_2O, $\delta_{C_7H_{16}}$ and δ_{H_2O}, are also shown for comparison. (c,f) Normalized species source terms *vs.* distance along the isocontour $T = T_{\text{peak}}$ for *n*-C_7H_{16} (solid blue) and H_2O (dashed red). (a-c) $Le = 1$; (d-f) $Le \neq 1$.

6. *

List of Tables

7. *

List of Figures